Biosensors and Bioelectronics 143 (2019) 111620

Contents lists available at ScienceDirect

Biosensors and Bioelectronics

journal homepage: www.elsevier.com/locate/bios

Developing a novel sensor based on ionic liquid molecularly imprinted polymer/gold nanoparticles/graphene oxide for the selective determination of an anti-cancer drug imiquimod

Moslem Afzali[a,b,*], Ali Mostafavi[a], Tayebeh Shamspur[a]

[a] Department of Chemistry, Shahid Bahonar University of Kerman, Kerman, Iran
[b] Young Researchers Society, Shahid Bahonar University of Kerman, Kerman, Iran

ARTICLE INFO

Keywords:
Imiquimod
Molecularly imprinted polymer
Au/GO composite
Glassy carbon electrode
Cyclic voltammetry
Square wave voltammetry

ABSTRACT

Despite its useful properties, imiquimod (IMQ), known as an anti-cancer drug, can be harmful to the skin at high concentrations. Therefore, we have developed a novel electrochemical sensor to determine IMQ, for the first time. A glassy carbon electrode (GCE) was modified by a new composite comprising of ionic liquid-based molecularly imprinted polymer (MIP) and gold nanoparticles/graphene oxide (Au/GO). The MIP/Au/GO nanocomposite was synthesized through non-covalent imprinting process in the presence of IMQ, as template molecule and characterized by SEM and FT-IR. The square wave voltammetry technique (SWV) was applied for IMQ determination in 0.1 M phosphate buffer solution (PBS) at pH 7.0. Several parameters affecting the IMQ quantification were evaluated and optimized. Under the optimized conditions, the sensor presented a linear range of 0.02–20.0 μM, a limit of quantification and detection of 0.02 μM and 0.006 μM, respectively. Low RSD values indicate the good repeatability and reproducibility of the modified electrodes in preparation and determination procedures. The satisfactory results indicated that the proposed sensor could be successfully applied for IMQ determination in real samples.

1. Introduction

IMQ (1-(2-Methylpropyl)-1H-imidazole[4,5-c]quinoline-4-amine) (Scheme S1), a member of the Imidazoquinolone family (Badavanis et al., 2018), is known as Human Papilloma Virus (HPV) drug (Camacho-Aguilar et al., 2018) and classified in the unique drugs category (Huang et al., 2019). It could stimulate the immune system (Emami et al., 2018) and is typically utilized as immunization agent for skin cancer treatment (Kang et al., 2018), actinic keratosis (Togsverd-Bo et al., 2018) and basal cell carcinoma (Bostanci et al., 2018). It is believed that this compound can fight the abnormal growth of skin cells (Wu et al., 2018). IMQ cream (5% w/w) has been developed for treating these diseases (Jansen et al., 2018; Kelati et al., 2018; Murray et al., 2018; Park et al., 2017). Topical drug delivery has several advantages including the avoidance of primary metabolism and gastrointestinal incompatibility (Sengupta and Chatterjee, 2017), improvement patient compliance (Read et al., 2017), the possibility of using a drug with short biological half-life and narrow therapeutic window (Freeman et al., 2018). Despite IMQ importance, it can be harmful to the skin in large amounts and cause local inflammatory reactions such as erythemas (Stockfleth et al., 2002). Thus, its measurement is essential, but so far, few methods were applied for its analysis such as high-performance liquid chromatography (HPLC) (Bachute and Turwale, 2013; Paula et al., 2008) and liquid chromatography/tandem mass spectrometry (Chan et al., 2011).

Molecularly imprinted polymers (MIPs) are a new class of materials with particular sites for specific molecules to selectively recognize target molecule (Zhu et al., 2018). These materials have recently received great attention, due to excellent selectivity, ease of preparation, and good stability (Ashley et al., 2017; Niu et al., 2016). However, using traditional monomers such as methacrylic acid and 4-vinyl pyridine, due to moderate binding kinetic and electrocatalytic activity is limited (Zhu et al., 2018). Ionic liquid (IL) monomers having high ionic conductivity, low vapor pressure, high thermal and chemical stability are good alternatives to them (Jia et al., 2018). MIPs have been synthesized through several methods (Díaz-Liñán et al., 2019; Sun et al., 2019), but the copolymerization of functional monomers and cross-linkers in the presence of template molecules is preferred. After the elimination of template, recognition sites are formed which are specific to molecules in terms of shape, size, and structure (Gui et al., 2018).

* Corresponding author.Imam Khomeini Highway- Pajuhesh square- Shahid Bahonar University of Kerman, the Faculty of Science, Department of Chemistry, Iran.
E-mail address: moslem_afzali@yahoo.com (M. Afzali).

https://doi.org/10.1016/j.bios.2019.111620
Received 29 May 2019; Received in revised form 3 August 2019; Accepted 19 August 2019
Available online 22 August 2019
0956-5663/

Herein, we reported an electrochemical sensor based on the GCE modified with ionic liquid-based MIP on the surface of Au/GO for IMQ determination. The combination of Au/GO and MIP led to increase the sensitivity and selectivity of this electrochemical sensor. MIP was synthesized using 1-allyl-3-vinylimidazolium bromide ($[VAIM]^+Br^-$) as functional monomer, ethylene glycol dimethyl acrylate (EGDMA) as a cross-linker and IMQ as the template molecule and through non-covalent polymerization.

2. Experimental

2.1. Apparatus

Electrochemical measurements were carried out using a PalmSens electrochemical analyzer driven by PSTrace 4.6 software (Palm Instruments, Houten, The Netherlands). A three-electrode configuration was utilized for all voltammetry analyses consisted of MIP/Au/GO/GCE as the working electrode, Ag/AgCl/KCl (3M) as the reference and a platinum wire as the axillary electrode. A Metrohm 827 pH meter (Herisau, Switzerland) was applied for pH measuring. A HPLC system (Model waters 600 E, U.S.A) equipped with a μBondapak C18 column (Waters, Ireland) [5.0 μm thickness, 3.9 mm × 300 mm], Rheodyne 7125i sampling valve with a 10 μL loop and an UV–vis detector (2487 waters) was employed to analyze the real samples. A mixture of acetonitrile/water 45:55 (%v/v) with a flow rate of 1.0 mL/min was used as the mobile phase. All voltammetry measurements were performed at room temperature.

A scanning electron microscopy (MIRA3, Tescan, Czech Republic) equipped with an energy-dispersive X-ray analyzer (EDX) was utilized for morphology investigations. The crystalline structure of the synthesized materials was studied by an X-ray diffraction system (Xpert MPD diffractometer, Philips, Netherlands). A Bruker Tensor FTIR apparatus (Poland) was applied to prepare FT-IR spectra. Transmission electron microscopy (TEM, EM-900, Zeiss, Germany) was used to study the structure of GO.

2.2. Reagents and solutions

IMQ (purity > 98%), $[VAIM]^+Br^-$ (purity ≥ 97%), EGDMA (98%), azobisisobutyronitrile (AIBN, 98%), chloroauric acid ($HAuCl_4{\cdot}4H_2O$), sodium citrate dihydrate ($Na_3C_6H_5O_7.2H_2O$), 1-ethyl-3-[3-dimethylaminopropyl] carbodiimide hydrochloride (EDC) and dimethyl sulfoxide (DMSO) were purchased from Sigma-Aldrich (Steinheim, Germany). The 5.0 mM standard solution of IMQ was daily prepared by dissolving it in DMSO, Graphite powder (< 300 μm, 99.99%), sulfuric acid (H_2SO_4, 98%), potassium permanganate ($KMnO_4$), hydrogen peroxide (H_2O_2), hydrochloric acid (HCl), sodium nitrate ($NaNO_3$), ethanol, sodium dihydrogen phosphate (NaH_2PO_4), disodium hydrogen phosphate (Na_2HPO_4) and phosphoric acid (H_3PO_4) (89%) were supplied from Merck (Darmstadt, Germany). Nafion (5% w/w) was purchased from Alfa Aesar (Ward Hill, MA, USA). 0.1 M PBS (pH 7.0) was prepared to use as the supporting electrolyte. Distilled water was utilized for chemical solution preparation. 100 mg placebo tablet and IMQ cream were supplied from Red Crescent (Iran, Kerman) and the pharmacy (Iran, Kerman), respectively.

2.3. Preparation of Au nanoparticles

Au NPs were prepared by the traditional chloroauric acid reduction method (Messaoud et al., 2017). 4 mL of $Na_3C_6H_5O_7.2H_2O$ solution (20 mM) was slowly added to 40 mL of the 1 mM aqueous solution of $HAuCl_4{\cdot}4H_2O$ on a heater-stirrer. The mixture was consecutively stirred at 70 °C until red color appears and then boiled for 15 min. Finally, the obtained product was transferred to ethanol to be stabilized.

2.4. Preparation of GO

GO was prepared according to our previous research (Afzali et al., 2019) using ultrapure graphite powder. Briefly, a mixture containing 4 g graphite, 100 mL H_2SO_4, and 4 g $NaNO_3$ was prepared, stirred for 2 h in an ice bath and then 12 g $KMnO_4$ was added to the mixture. After 6 h stirring at 35 °C, the mixture was cooled to the room temperature and 10 mL 30% H_2O_2 was added to it. The obtained product was centrifuged, washed with 30% HCl and deionized water three times, and dried in an oven at 60 °C for 24 h.

2.5. Preparation of MIP/Au/GO

First, we prepared the Au/GO nanocomposite as follows: 30 mg of GO was dispersed in 10 mL ethanol by 30 min sonicating. The dispersion should be treated through a 0.2 M EDC solution for 10 h to activate the carboxylate groups of GO. After that, 10 mL of Au suspension (2 mg mL^{-1}) was added to it and vigorously stirred for 2 h to obtain Au/GO nanocomposite. The product was collected, washed, and dried at 60 °C for 8 h.

Afterward, MIP/Au/GO was prepared by the non-covalent imprinting process, which depends on forming interactions between the functional monomer and template in a pre-polymerization mixture (Ashley et al., 2017). 0.8 mmol $[VAIM]^+Br^-$ as the functional monomer and 0.2 mmol IMQ as the template molecule were added to 10 mL solvent (ethanol/water, 4:1 v/v). When $[VAIM]^+Br^-$ was dissolved entirely, 25 mL GO suspension (3 mg mL^{-1}), 4 mmol EGDMA as the cross-linker agent and 10 mg azobisisobutyronitrile (AIBN) as the initiator were added to the solution. This mixture was sonicated for 20 min, then purged with nitrogen for 15 min to remove oxygen and finally, allowed to polymerize at 60 °C for 24 h. To remove template molecules, the obtained particles were repeatedly washed with acetic acid/methanol (9:1, v/v) through centrifugation (4000 rpm) until HPLC did not detect IMQ. The MIP/Au/GO composite was finally dried in vacuum at 60 °C for 8 h. Non-imprinted polymer (NIP) was synthesized in the same conditions, just in the absence of template molecule in the polymerization process.

2.6. Fabrication of the modified glassy carbon electrode

The GCE was polished with 0.3 and 0.05 μm alumina slurry and washed with distilled water. Then it was sonicated in ethanol for 5 min until a mirror-like surface was obtained. 10 mg of MIP/Au/GO nanocomposite was ultrasonically dispersed in 2 mL methanol, then 10 μL of the dispersion was mixed with 10 μL 5% w/w nafion, as the binder. Finally, 2 μL of the suspension was dropped onto the surface of the GCE and left to dry at room temperature for 1 h. The fabricated sensor was named MIP/Au/GO/GCE and employed to measure IMQ with CV and SWV according to the general procedure.

2.7. Preparation of the real samples

For sample preparation, one tablet was pulverized, and a specified weight of powder was dissolved in distilled water. The filtration was performed and undissolved contents were removed. So, the residual solution was collected in a 100 ml volumetric flask, and 1.0 mL of it was added to 9.0 mL of 0.1 M PBS (pH 7.0) in an electrochemical cell. 1.60 mg of IMQ cream (equivalent to 3.5 μM) was weighted and transferred to 100 mL voltammetric flask. DMSO as the diluent, was added to cream and sonicated for 60 min. 5.0 mL of the solution was added to 5.0 mL of 0.1 M PBS, and its electrochemical behavior was investigated.

2.8. Experimental procedure

10 mL of 0.1 M PBS (pH 7.0) was transferred into the

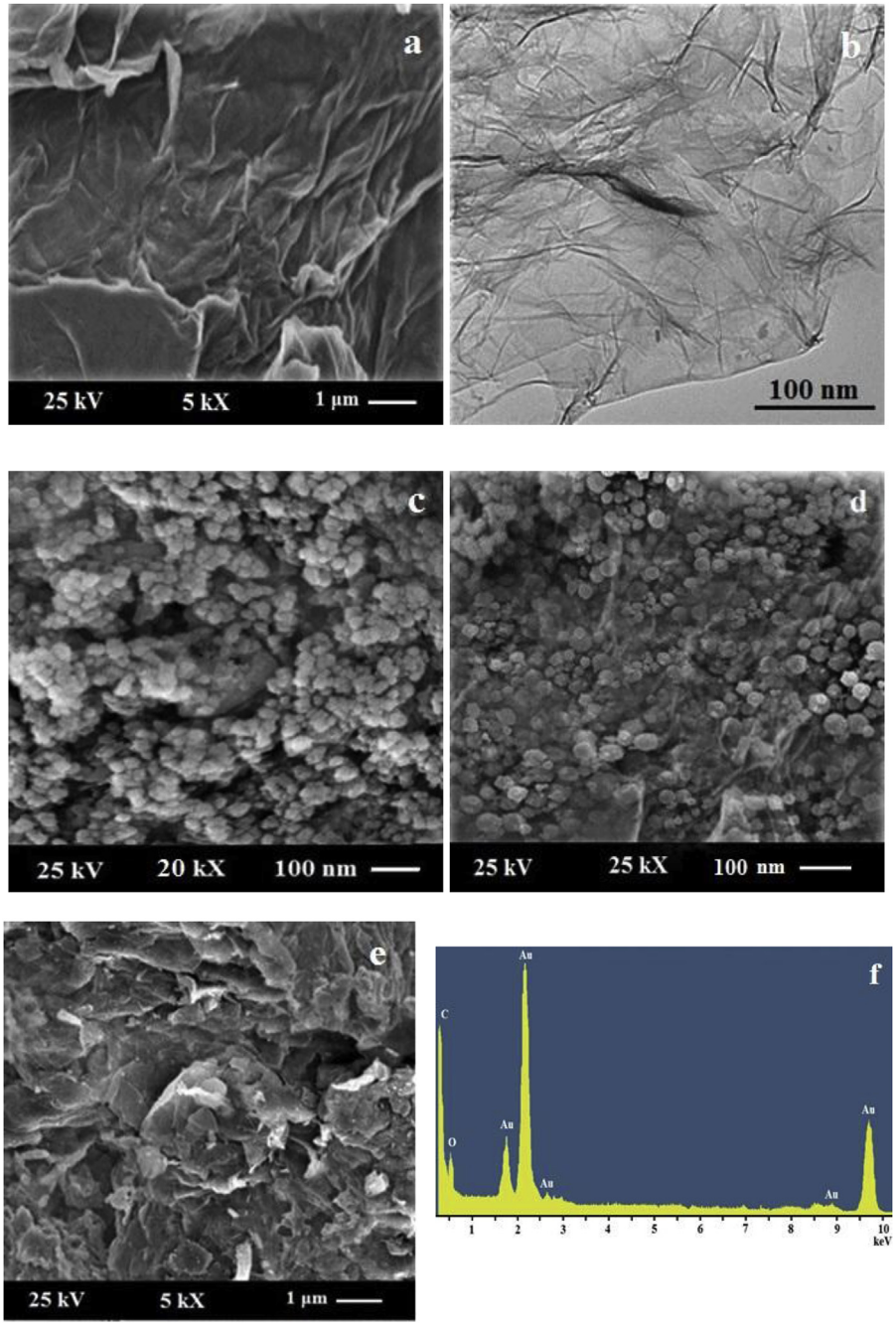

Fig. 1. a) SEM image of GO, b) TEM image of GO, c) SEM image of Au nanoparticles, d) SEM image of Au/GO, e) SEM image of MIP/Au/GO, f) EDX analysis of Au/GO.

electrochemical cell and then 15.0 µM of IMQ solution was added to it by a micropipette. The IMQ solutions prepared at similar conditions were continuously stirred at 400 rpm and 37 °C for different times (2, 5, 10 and 15 min). Since IMQ is slightly soluble in water, it takes at least 10 min to the solution be homogenized, so, 10 min was selected as the optimum time for stirring the solution. Afterward, the solution kept quiet for 15 s. The prepared electrodes were put in the solution and IMQ measurement was performed by CV and SWV. Square wave voltammograms (SWVs) were recorded in the potential range of 0.5 V–1.3 V at the scan rate of 50 mV s^{-1}, the step potential of 4 mV, the pulse amplitude of 25 mV and the frequency of 15 Hz as instrumental parameters.

3. Results and discussion

3.1. Characterization

The GO morphology was characterized by SEM, and as shown in Fig.1a, a wrinkled structure with the irregular surface was observed which is typical of GO. The TEM image in Fig. 1b also confirms the layered structure of GO with thin layers and irregular shapes where the overlapping of some layers is also observed. Fig. 1c, the SEM image of Au nanoparticles, illustrates that spherical and mostly uniform nanoparticles were formed during the synthesis process with an average diameter of 38 nm. Fig. 1d presents the SEM image of Au/GO nanocomposite and clearly shows that spherical Au nanoparticles are uniformly dispersed on the GO sheets surface. The SEM image of the MIP/

Au/GO nanocomposite (Fig. 1e) demonstrates that the GO surface morphology did not change after polymerization, just became slightly rough. These observations are in agreement with the results previously reported and confirm the composite formation (Chen and Ye, 2017).

The prepared materials structure was studied by XRD, and the results are illustrated in Fig. S1 (supplementary information data). The diffraction peak of GO located at 2θ = 12.9° is attributed to (002) plane (Wei et al., 2017), while the characteristic peak of graphite has appeared at 2θ = 25.8° (Lavi et al., 2019). The interlayer spacing of GO is about 0.85 nm, and this higher d-spacing value compared to that of graphite (0.35 nm) confirms that graphite was successfully oxidized and oxygen-containing functional groups had been introduced to layers. In the XRD pattern of Au nanoparticles in Fig. S1, characteristic peaks of (111), (200), (220), (311) and (222) planes are observed at 2θ = 37.8°, 44.6°, 64.9°, 76.9° and 82.1°, respectively which confirm the Au formation (JCPDS file: 04–0784). The XRD pattern of Au/GO nanocomposite is also presented in Fig. S1, and illustrates the characteristic peak of GO, as well as two sharp peaks at 38.0° and 44.9° which could be assigned to (111) and (200) faces of the Au nanoparticles on the surface of GO.

Furthermore, the chemical structure of GO and MIP/Au/GO were also investigated by FT-IR and the results are shown in Fig. S2. The characteristic peaks of 1051, 1226, 1625, 1732 and 3400 cm^{-1} attributed to C–O, C–OH, C = C, C = O and O–H stretching vibrations, respectively confirm the formation of GO through the oxidation of graphite (Singu and Yoon, 2018). The FT-IR spectrum of the MIP/Au/GO nanocomposite shows the characteristic peaks of MIP, as well as Au/GO and approves the presence of all components in the composite. A broad peak at 3400 cm^{-1} attributed to the stretching mode of O–H group and the peaks at 1191 cm^{-1} and 1028 cm^{-1} are assigned from the C–N stretching bands of the imidazolium ring. The C = N stretching band which is the signature of the imidazolium ring was appeared at 1632 cm^{-1} and C–H vibrations are also observed at 2916 and 2844 cm^{-1}. The peaks at 1732 and 1625 are due to the C = O and C = C stretching modes, respectively (Zhu et al., 2018).

3.2. The electrochemical behavior of the modified electrode in IMQ determination

First, we evaluated the bare GCE in the absence of IMQ in 0.1 M PBS (pH 7.0) and it was found that there was no oxidation peak (Orange peak in Fig. 2). Afterward, the background-subtracted SWVs of 20 μM IMQ in 0.1 M PBS (pH 7.0) were recorded in the presence of bare GCE, GO/GCE, Au/GO/GCE, MIP/Au/GO/GCE and NIP/Au/GO/GCE and compared with the bare GCE (Fig. 2). The bare GCE (light blue peak) showed a low oxidation current of IMQ. By modifying the GCE with GO (purple curve), the sensitivity was significantly increased due to the GO existence and its excellent conductivity (Wei et al., 2017). At the Au/GO/GCE (green curve), due to the electrocatalytic activity of Au nanoparticles (Rassas et al., 2019), the rate of electron transfer was increased, and the over-potential of IMQ oxidation was reduced. The MIP/Au/GO/GCE (red curve) illustrated that the sensitivity is slightly decreased. We attribute the high peak current of the MIP to its cavities, as IMQ could pass through these cavities and reach the surface of the electrode more easily (Xing et al., 2012). When we used NIP/Au/GO/GC (dark blue) in the same conditions, the anodic peak current of IMQ was severely reduced (Xing et al., 2012), and just a slight increase in sensitivity was observed in comparison with the bare GCE. It can be concluded that the formed polymer matrix covers the surface of Au/GO and block electron transfer (Kumar et al., 2018).

3.3. The effect of scan rate

To evaluate the electro-oxidation process of 10.0 μM IMQ, the anodic peak current (Ip_a) and peak potential (E_p) were studied at different scan rats (2–100.mV s^{-1}) by CV using MIP/Au/GO/GCE in 0.1 M PBS. The results (Fig. 3) showed that by increasing the scan rate, the anodic peak current was increased without any change or shift to more positive values. The linear relationship between the IMQ oxidation peak current and the square root of scan rates (inset a) suggests that the IMQ oxidation process was controlled by diffusive process, while by increasing scan rate (ν), current went out of the linear state (inset b).

3.4. Type and pH of buffer solution

Various buffer solutions including 0.1M Robinson, phosphate, acetate, and borate with the concentration of 0.1 M were tested and the obtained results are shown in Fig. S3. According to the results, the highest anodic peak current of IMQ was obtained by using PBS, so, it was selected for next experiments. PBS pH, as an active parameter in electrochemical investigations, should be optimized. As shown in Fig. S4, SWVs of 20.0 μM IMQ in 0.1 M PBS were studied at pH range of 3.0–9.0. The results demonstrate that by increasing pH from 3.0 to 9.0 (right to the left), the oxidation peak potential changes toward more negative amounts. The best pH for the IMQ quantification was found to be 7.0 and selected for the next experiments. The inset of Fig. S4 shows

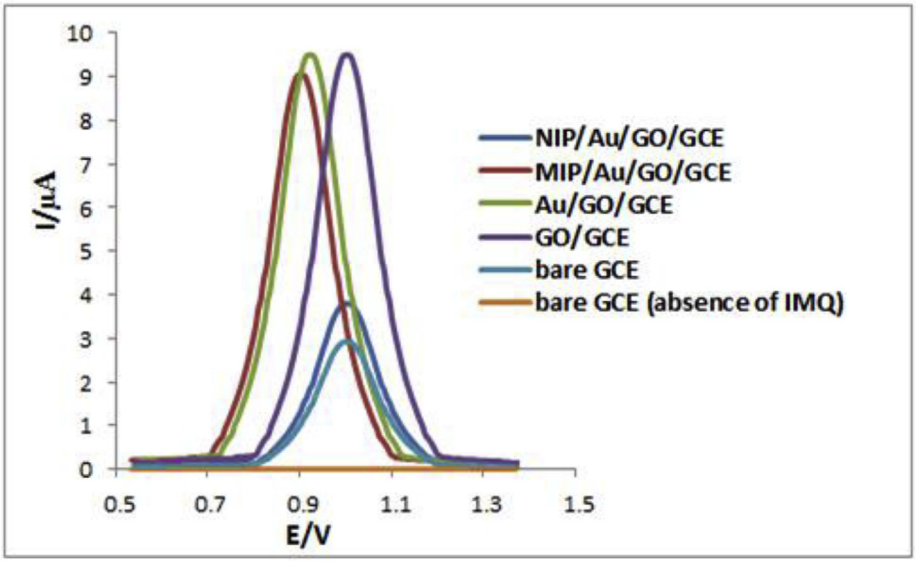

Fig. 2. The SWVs of 20 μM IMQ in 0.1 M PBS (pH 7.0) at the bare GCE and modified electrodes at the scan rate of 50 mVs^{-1}.

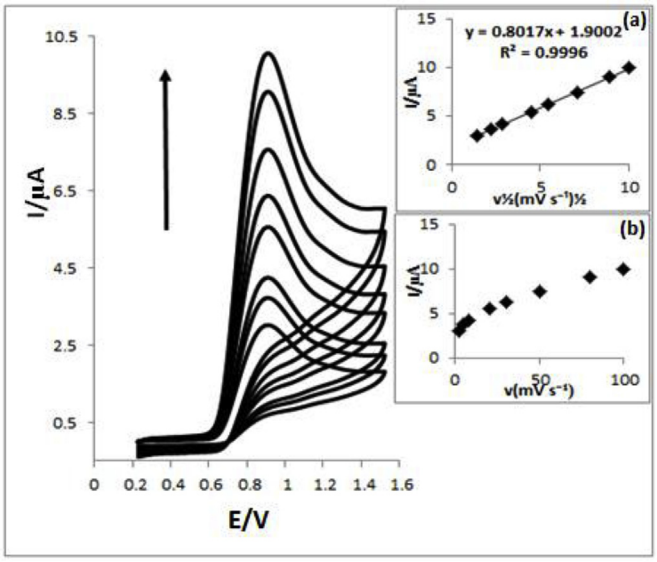

Fig. 3. The cyclic voltammograms (CVs) of IMQ in 0.1 M PBS (pH 7.0) by MIP/Au/GO/GCE at different scan rates (2, 5, 8, 20, 30, 50, 80 and 100 mV s^{-1}). Inset: (a) The relationship between the oxidation peak current and the square root of scan rate ($\nu^{1/2}$), (b) scan rates (ν).

the linear relationship between peak potential (E_p) and pH with the correlation coefficient (R^2) of 0.9972. The theoretical equation related to E_p and pH is $E_p = (-0.0592\,m/n)$ pH + b, where m and n are the numbers of transferred protons and electrons involved in the electrochemical procedure. The curve slope extracted from the equation of $E_p = -0.0568$ pH + 1.3036 was obtained -0.0568 V/pH, which is closed to the theoretical value. It has been previously demonstrated that the oxidation mechanism of adenine which has the same structure as IMQ could involve the equal transferred electrons and protons in the electrochemical process, as depicted in Scheme 1 (Choi et al., 2017).

3.5. Analytical performance

The SWVs of IMQ were evaluated at different concentrations (0.02–20.0 μM) in 0.1 M PBS (pH 7.0) at the MIP/Au/GO/GCE. As illustrated in Fig.4a, the oxidation peak current of IMQ was gradually increased by increasing concentration from 0.02 μM to 20.0 μM. Fig. 4 inset shows that there is a linear relationship between the anodic peak current and various concentrations of IMQ (R^2 = 0.9991). LOQ and LOD were calculated from $10S_b/m$ and $3S_b/m$ equation, where S_b is the standard deviation of the blank sample and m is the slope of the calibration plot, and obtained 0.006 μM and 0.02 μM, respectively. Standard error bars of repeatability/reproducibility for different concentrations of IMQ (0.02–20.0 μM) were investigated and are shown in Fig. 4 (b, c) and Tables S1 and S2. The results displayed the variability of means of six replicated and reproduced analysis with the relative standard deviations (RSDs) of 4.4%–0.8% and 6.2 to 0.9%, respectively. Low RSDs demonstrated good repeatability and reproducibility of the modified electrodes in the preparation and determination procedure.

The stability of the modified GCE was investigated by multi-scan CV according to the general procedure. Fig. S5 indicates that after 60 cycles, CVs showed no change with a deviation of more than 10%. The storage stability test of the proposed sensor for 20.0 μM IMQ was performed two times (i) immediately after the preparation of the electrode and (ii) after 30 days. The electrode was kept and stored in the refrigerator at 4 °C during this time. After 30 days, the anodic response of the sensor was still retained 98.5% of the initial response value, which demonstrates the good long-term stability of the proposed modified electrode.

3.6. The evaluation of interfering compounds

Under the optimized conditions, some compounds with a similar structure to IMQ such as quinolone, imidazole, adenine, guanine and uric acid were tested as interfering species. The results are shown in Table S3. It could be seen that by adding 500-fold of organic compounds to 20.0 μM IMQ, no significant change in the oxidation peak current of IMQ was observed. So, recoveries caused an error of less than ± 5% for IMQ determination. The SWVs of 20.0 μM solution of adenine and guanine simultaneously studied with 20.0 μM IMQ are shown in Fig. S6. Accordingly, the oxidation peak potential of guanine, adenine, and IMQ took place at 0.7 V, 0.8 V and 0.9 V, respectively due to their molecular structures. Previously, adenine and guanine were measured simultaneously, and it was demonstrated that the oxidation of guanine appeared at more positive potential values than guanine (Oliveira-Brett et al., 2002). The results showed that these molecules did not significantly change the anodic peak current and potential of IMQ.

3.7. The quantification of IMQ in real samples

Placebo pharmaceutical sample and IMQ cream were studied as real samples. Placebo is an inert substance and has no impact on the disease itself; it can only affect the person's perception of their condition (Micozzi, 2018). Fig. S7 shows the SWVs of placebo and IMQ-added placebo sample in which the concentration of IMQ is rising. Since placebo showed no oxidation peak current, it can be concluded that it is an inert drug (Crawford et al., 2015) and the IMQ-added placebo sample was easily measured without any disturbance in real placebo

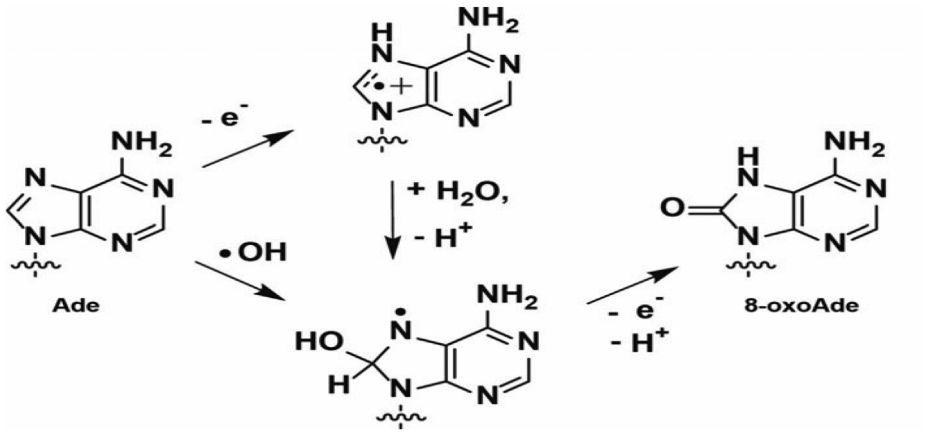

Scheme 1. The electro-oxidation of adenine as the same structure as IMQ.

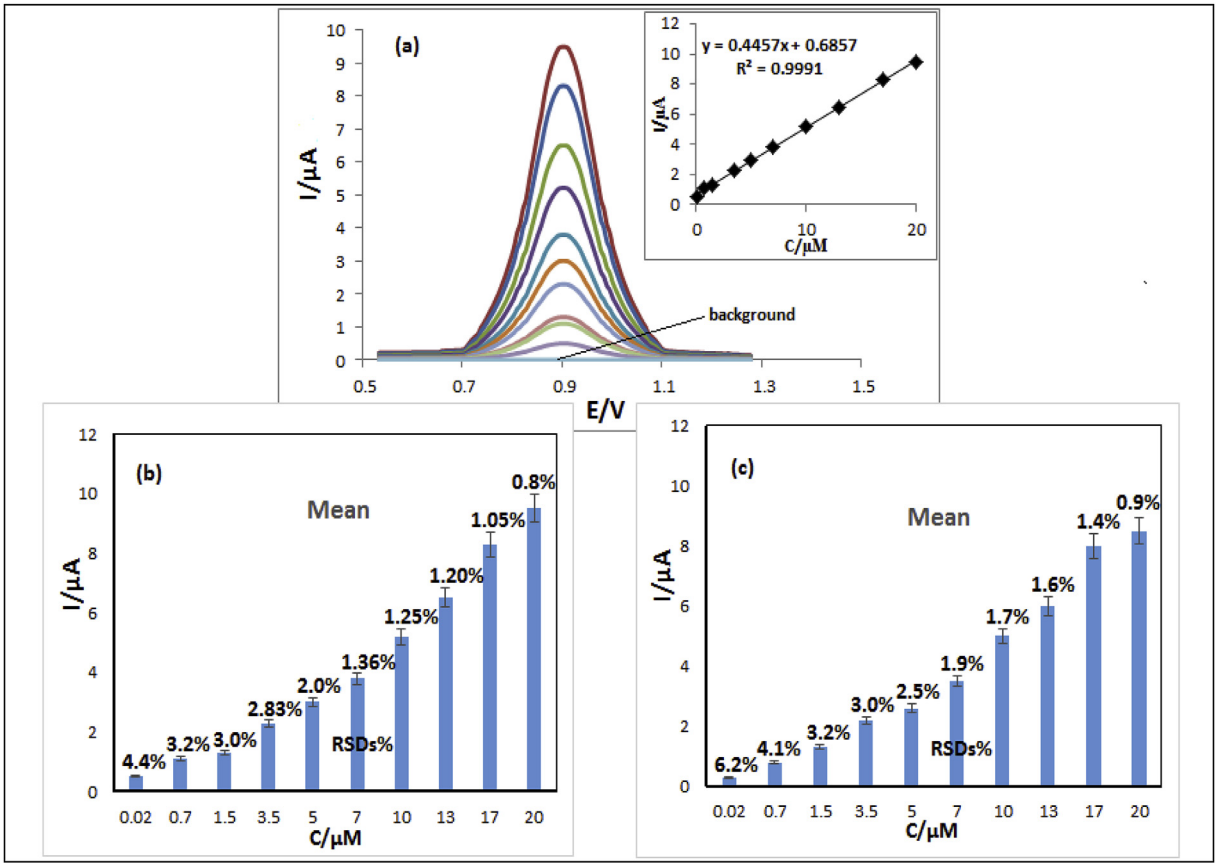

Fig. 4. (a) SWVs at various concentrations of IMQ (down to up: 0.02, 0.70, 1.50, 3.50, 5.00, 7.00, 10.0, 13.0, 17.0 and 20.0 μM) in 0.1 M PBS (pH 7.0) at MIP/Au/GO/GCE. Inset: the linear relationship between anodic peak currents and different concentrations of IMQ. Instrumental parameters: scan rate 50 mV s^{-1}, step potential 4 mV, pulse amplitude 25 mV and frequency 15 Hz. (b) The repeatability bar graph of method responses from the same electrodes, (c) The reproducibility bar graph of method responses from six different electrode preparations (Error bars indicates standard deviation for n = 6).

Table 1
Determination of IMQ in placebo pharmaceutical sample and IMQ cream.

Sample	Certified amount	**Added amount (μM)**	**Found amount** [a] **(μM)**	RSD (%)	Relative recovery (%)	**Found HPLC method (μM)**	F_{tab} $^{(0.05;95\%)}$	F_{exp}	$t_{tab\ (98\%)}$	t_{exp}
Placebo tablet	100 (mg per-tablet)	–	0.00	–	–	0.00	–	–	–	–
		3.50	3.51 ± 0.05	1.42	100.2	3.47 ± 0.1	19.0	4.0	3.8	0.85
		10.0	10.2 ± 0.03	0.29	101.0	9.70 ± 0.08	19.0	7.11	3.8	2.35
IMQ cream	3.50 μM	–	3.48 ± 0.06	1.72	99.42	3.40 ± 0.15	19.0	6.25	3.8	1.95
		1.50	5.00 ± 0.04	0.80	101.3	4.46 ± 0.11	19.0	7.56	3.8	2.48
		10.0	13.50 ± 0.02	0.14	100.2	13.0 ± 0.07	19.0	12.25	3.8	3.00

[a] Mean ± standard deviation (n = 3).

Table 2
Comparison of the present method with the HPLC previously reported for the quantification of IMQ.

Detection method	Linear range	LOQ	Ref
HPLC-PDA[a]	40.0–62.0 μM	–	Bachute and Turwale (2013)
HPLC-UV	0.41–10.0 μM	0.41 μM	Paula et al. (2008)
Square wave voltammetry	0.02–20.0 μM	0.02 μM	This work

[a] HPLC-Photo diode array.

sample. Standard addition was performed for two samples with specific amounts of IMQ. Satisfactory results of RSD and relative recovery indicated good precision and accuracy (Table 1). Also, the F-test and *t*-test, which indicate the precisions and accuracy of the method respectively, were utilized for comparing the obtained results of the proposed method with that of HPLC-UV method in two real samples. According to the results, no significant difference between the results of two methods was observed which confirms that the proposed method is applicable for precise and accurate determination of IMQ in placebo pharmaceutical and cream samples.

F_{tab} is the F value obtained from the one-tailed Table of F-test; t_{tab} is the t-value obtained from the table of student t-test. F_{exp} and t_{exp} are calculated F-value and t-value, respectively.

3.8. Comparison of the present method with previous reports

The performance of the present method for IMQ determination was compared with previously reported methods (Bachute and Turwale, 2013; Paula et al., 2008). Table 2 clearly shows that this method has a more extensive linear range and lower detection limit compared to HPLC methods. So, this sensor can be successfully applied for IMQ

determination as an inexpensive, simple, and selective method.

4. Conclusions

In this work, we have developed a novel electrochemical sensor for the selective and sensitive voltammetric determination of IMQ, in which a three-component nanocomposite consists of an ionic liquid-based MIP, Au nanoparticles and GO nanosheets was successfully cast on the surface of a GCE. The presence of GO significantly enhances the sensitivity of the sensor, due to the electrical conductivity of GO, and MIP with particular sites for IMQ recognition improves the sensor selectivity. Besides, the proposed sensor exhibits good linearity, repeatability, reproducibility, and stability. The lowest IMQ concentration, which was detectable by this sensor was obtained to be 0.006 μM. It also possessed an enhanced electrocatalytic activity, a simple fabrication procedure, and fast response. The method was successfully applied for IMQ detection in real samples with satisfactory results. Briefly, the proposed sensor in this study introduces an easy and reliable process for IMQ determination and also provides a progressive route for designing novel and selective electrochemical sensors to detect other molecules using MIPs.

CRediT authorship contribution statement

Moslem Afzali: Conceptualization, Methodology, Software, Writing - original draft. **Ali Mostafavi:** Supervision. **Tayebeh Shamspur:** Writing - review & editing, Supervision.

Declaration of Competing Interest

The authors declare that they have no known competing financial interests or personal relationships that could have appeared to influence the work reported in this paper.

Acknowledgment

The authors would like to express their sincere appreciation to the founders of the Shahid Bahonar University of Kerman, Mr. Alireza Afzalipour and his wife, Mrs. Fakhereh Saba, for their foresight and generosity in training future generations of doctors, engineers and scientists. Also, the authors would like to acknowledge their thanks to Dr. Parviz Dabiri for his generous support for the research activities of the chemistry and nano laboratories in the Shahid Bahonar University of Kerman.

Appendix A. Supplementary data

Supplementary data to this article can be found online at https://doi.org/10.1016/j.bios.2019.111620.

References

Camacho-Aguilar, S., Ramírez-Amador, V., Rosendo-Chalma, P., Guido-Jiménez, M., García-Carrancá, A., Anaya-Saavedra, G., 2018. Oral Dis. 24 (1–2), 210–214.
Togsverd-Bo, K., Halldin, C., Sandberg, C., Gonzalez, H., Wennberg, A., Sørensen, S., Wulf, H., Hædersdal, M., 2018. Br. J. Dermatol. 178 (4), 903–909.
Afzali, M., Mostafavi, A., Shamspur, T., 2019. D. Talanta 196, 92–99.
Ashley, J., Shahbazi, M.-A., Kant, K., Chidambara, V.A., Wolff, A., Bang, D.D., Sun, Y., 2017. Biosens. Bioelectron. 91, 606–615.
Bachute, M.T., Turwale, S.L., 2013. J. Pharm. Res. 6 (1), 73–77.
Badavanis, G., Pasmatzi, E., Monastirli, A., Tsambaos, D., 2018. Case Rep. Clin. Med. 7 (01), 1.
Bostanci, S., Kocyigit, P., Vural, S., Heper, A.O., Botsali, A., 2018. Dermatol. Surg. 44 (1), 36–41.
Chan, D., Tarbin, J., Sharman, M., Carson, M., Smith, M., Smith, S., 2011. Anal. Chim. Acta 700 (1–2), 194–200.
Chen, X., Ye, N., 2017. RSC Adv. 7 (54), 34077–34085.
Choi, Y.J., Chang, S.J., Gibala, K.S., Resendiz, M.J., 2017. Chem. Eur J. 23 (28), 6706–6716.
Crawford, M.J., Sanatinia, R., Barrett, B., Byford, S., Cunningham, G., Gakhal, K., Lawrence-Smith, G., Leeson, V., Lemonsky, F., Lykomitrou, G., 2015. Trials 16 (1), 308.
Díaz-Liñán, M., López-Lorente, A., Cárdenas, S., Lucena, R., 2019. Sens. Actuators B Chem. 287, 138–146.
Emami, T., Rezayat, S.M., Khamesipour, A., Madani, R., Habibi, G., Hojatizade, M., Jaafari, M.R., 2018. Artif Cell Nanomed B. pp. 1–10.
Freeman, W., Sailor, M.J., Cheng, L., Cunin, F., Anglin, E., Li, Y.Y., 2018. U.S. Pat. Application 15/804, 856.
Gui, R., Jin, H., Guo, H., Wang, Z., 2018. Biosens. Bioelectron. 100, 56–70.
Huang, X., Yu, P., Liu, M., Deng, Y., Dong, Y., Liu, Q., Zhang, J., Wu, T., 2019. Int. Immunopharmacol. 66, 236–241.
Jansen, M.H., Mosterd, K., Arits, A.H., Roozeboom, M.H., Sommer, A., Essers, B.A., van Pelt, H.P., Quaedvlieg, P.J., Steijlen, P.M., Nelemans, P.J., 2018. J. Investig. Dermatol. 138 (3), 527–533.
Jia, M., Yang, J., Sun, Y.K., Bai, X., Wu, T., Liu, Z.S., Aisa, H.A., 2018. Anal. Bioanal. Chem. 410 (2), 595–604.
Kang, A., Zhao, D., Yeh, J.J., Lee, D.J., 2018. Curr Dermatol Rep 7 (4), 311–320.
Kelati, A., Khemis, A., Montaudié, H., Lacour, J.P., Passeron, T., 2018. J. Am. Acad. Dermatol. 79 (4), 758–760.
Kumar, S., Karfa, P., Madhuri, R., Sharma, P.K., 2018. J. Phys. Chem. Solids 116, 222–233.
Lavi, O., Haik, O., Hirshberg, D., Talyosef, Y., Zinigard, E., Markovsky, B., Elias, Y., Aurbach, D., Kovacheva, D., 2019. Carbon.
Messaoud, N.B., Ghica, M.E., Dridi, C., Ali, M.B., Brett, C.M., 2017. Sensoe Actuat B-Chem. Chemical 253, 513–522.
Micozzi, M.S., 2018. Fundamentals of Complementary, Alternative, and Integrative Medicine. E-Book, pp. 98.
Murray, M.L., Meadows, J., Doré, C.J., Copas, A.J., Haddow, L.J., Lacey, C., Jit, M., Soldan, K., Bennett, K., Tetlow, M., 2018. BMC Med. Res. Methodol. 18 (1), 125.
Niu, M., Pham-Huy, C., He, H., 2016. Microchem Acta 183 (10), 2677–2695.
Oliveira-Brett, A., Diculescu, V., Piedade, J., 2002. Bioelectrochemistry 55 (1–2), 61–62.
Park, A.J., Paul, J., Chapman, M.S., Samie, F.H., 2017. Dermatol. Surg. 43 (8), 1017–1022.
Paula, D.D., Martins, C.A., Bentley, M.V.L.B., 2008. Biomed. Chromatogr. 22 (12), 1416–1423.
Rassas, I., Braiek, M., Bonhomme, A., Bessueille, F., Raffin, G., Majdoub, H., Jaffrezic-Renault, N., 2019. Sensors 19 (1), 154.
Read, T., Webber, S., Thomas, J., Wagels, M., Schaider, H., Soyer, H.P., Smithers, B.M., 2017. BMJ open 7 (10), e016816.
Sengupta, P., Chatterjee, B., 2017. Int. J. Pharm. 526 (1–2), 353–365.
Singu, B.S., Yoon, K.R., 2018. Electrochim. Acta 268, 304–315.
Stockfleth, E., Meyer, T., Benninghoff, B., Salasche, S., Papadopoulos, L., Ulrich, C., Christophers, E., 2002. Arch. Dermatol. 138 (11), 1498–1502.
Sun, Y., Xu, L., Waterhouse, G.I., Wang, M., Qiao, X., Xu, Z., 2019. Sens. Actuators B Chem. 281, 107–114.
Wei, X., Xu, X., Qi, W., Wu, Y., Wang, L., 2017. Pro Nat Sci-Mater. 27 (3), 374–379.
Wu, R., Liao, Y., Shen, W., Liu, Y., Zhang, J., Zheng, M., Chen, G., Su, Y., Zhao, M., Lu, Q., 2018. Mol. Med. Rep. 18 (4), 3973–3982.
Xing, X., Liu, S., Yu, J., Lian, W., Huang, J., 2012. Biosens. Bioelectron. 31 (1), 277–283.
Zhu, X., Zeng, Y., Zhang, Z., Yang, Y., Zhai, Y., Wang, H., Liu, L., Hu, J., Li, L., 2018. Biosens. Bioelectron. 108, 38–45.